Available online at www.sciencedirect.com
SCIENCE DIRECT®
Journal of Solid State Chemistry 177 (2004) 26–37
JOURNAL OF SOLID STATE CHEMISTRY
http://elsevier.com/locate/jssc

Transport properties and stability of Ni-containing mixed conductors with perovskite- and K_2NiF_4-type structure

V.V. Kharton,[a,b,*] A.A. Yaremchenko,[a] A.L. Shaula,[a] M.V. Patrakeev,[c] E.N. Naumovich,[b] D.I. Logvinovich,[b] J.R. Frade,[a] and F.M.B. Marques[a]

[a] *Department of Ceramics and Glass Engineering, CICECO, University of Aveiro, 3810-193 Aveiro, Portugal*
[b] *Institute of Physicochemical Problems, Belarus State University, 14 Leningradskaya Str., 220050 Minsk, Republic of Belarus*
[c] *Institute of Solid State Chemistry, Ural Division of RAS, 91 Pervomayskaya Str., Ekaterinburg 620219, Russia*

Received 9 March 2003; received in revised form 25 April 2003; accepted 7 May 2003

Abstract

The total conductivity and Seebeck coefficient of a series of Ni-containing phases, including $La_2Ni_{1-x}M_xO_{4+\delta}$ (M = Co, Cu; x = 0.1–0.2) with K_2NiF_4-type structure and perovskite-like $La_{0.90}Sr_{0.10}Ga_{0.65}Mg_{0.15}Ni_{0.20}O_{3-\delta}$ and $La_{0.50}Pr_{0.50}Ga_{0.65}Mg_{0.15}Ni_{0.20}O_{3-\delta}$, were studied in the oxygen partial pressure range from 10^{-18} Pa to 50 kPa at 973–1223 K. Within the phase stability domain, the conductivity of layered nickelates is predominantly p-type electronic and occurs via small-polaron mechanism, indicated by temperature-activated hole mobility and $p(O_2)$ dependencies of electrical properties. In oxidizing conditions similar behavior is characteristic of Ni-containing perovskites, which exhibit, however, significant ionic contribution to the transport processes. The role of ionic conduction increases with decreasing $p(O_2)$ and becomes dominant in reducing atmospheres. All nickelate-based phases decompose at oxygen pressures considerably lower with respect to Ni/NiO boundary. The partial substitution of nickel in $La_2Ni(M)O_{4+\delta}$ has minor effect on the stability limits, which are similar to that of $La_{0.90}Sr_{0.10}Ga_{0.65}Mg_{0.15}Ni_{0.20}O_{3-\delta}$. On the contrary, praseodymium doping enhances the stability of $La_{0.50}Pr_{0.50}Ga_{0.65}Mg_{0.15}Ni_{0.20}O_{3-\delta}$ down to $p(O_2)$ values as low as 10^{-17}–10^{-10} Pa at 1023–1223 K.

Keywords: Lanthanum nickelate; Perovskite; K_2NiF_4-type structure; Phase stability; Total conductivity; Seebeck coefficient; Mixed conductor; Electron–hole transport; Oxygen permeability

1. Introduction

Due to potential high environmental and economic impact, dense ceramic membranes with mixed oxygen-ionic and electronic conductivity attract significant interest for conversion of light hydrocarbons in electrocatalytic membrane reactors, particularly for partial oxidation of methane to syngas [1–3]. One promising group of membrane materials relates to phases derived from lanthanum nikelates with perovskite- and K_2NiF_4-type structure, showing a substantially high level of oxygen permeability [4–12]. High catalytic activity of nickel in oxidation reactions [13,14] makes it possible to expect an improvement in the conversion efficiency when using Ni-containing membranes.

The oxide phases existing in ternary La–Ni–O system include perovskite-type $LaNiO_{3-\delta}$ and Ruddlesden–Popper series $La_{n+1}Ni_nO_{3n+1}$, with $La_2NiO_{4+\delta}$ having a K_2NiF_4-type structure as the end-member ($n = 1$). Oxygen-deficient $LaNiO_{3-\delta}$ exhibits a metallic conductivity, which is as high as about 10^3 S/cm at room temperature [12,15] and can be attributed to a transformation of σ-bonding e_g orbitals of low-spin Ni^{3+} into itinerant σ^*-band states [16]. $LaNiO_{3-\delta}$ exists, however, in a narrow range of temperatures and oxygen partial pressures; in air this phase decomposes into $La_{n+1}Ni_nO_{3n+1}$ and NiO at temperatures above 1100 K [12,17,18]. The perovskite phase stability domain can be enlarged by extensive B-site doping, such as substitution of nickel with gallium [10–12]. The perovskite-type

*Corresponding author. Present address: Department of Ceramics and Glass Engineering, CICECO, University of Aveiro, 3810-193 Aveiro, Portugal. Fax: +351-234-370263.
E-mail address: kharton@cv.ua.pt (V.V. Kharton).

0022-4596/03/$ - see front matter © 2003 Elsevier Inc. All rights reserved.
doi:10.1016/S0022-4596(03)00261-5

$LaNi_{1-x}Ga_xO_{3-\delta}$, stable at $x \geqslant 0.5$, possess relatively high oxygen permeability limited by vacancy diffusion [10,11]. Further acceptor-type doping, particularly incorporation of strontium into the *A* sublattice and magnesium into the *B* sites, results in increasing oxygen-vacancy concentration and, consequently, oxygen permeation fluxes [7,19]. This is accompanied, however, with increasing role of oxygen exchange kinetics on the membrane surface as a permeation-limiting factor. Nonetheless, the permeability of perovskite-type $LaGa_{0.65}Mg_{0.15}Ni_{0.20}O_{3-\delta}$ and its derivatives, $La_{1-x}A_xGa_{0.65}Mg_{0.15}Ni_{0.20}O_{3-\delta}$ (A = Sr, Pr; x = 0.1–0.5), is higher compared to La(Sr)Fe(Co)$O_{3-\delta}$ [7,19].

The $La_2NiO_{4+\delta}$ phase is oxygen-hyperstoichiometric, a result of incorporation of interstitial oxygen anions into the rock-salt layers of intergrowth K_2NiF_4-type structure. In air, the equilibrium oxygen nonstoichiometry is 0.14–0.16 at 300 K and decreases on heating [4,20–23]. At temperatures below 600 K, $La_2NiO_{4+\delta}$ exhibits a semiconductor-type electronic conductivity, which occurs via hopping of p-type charge carriers between mixed-valence nickel cations; a smooth change to metallic-like conduction is observed at higher temperatures [21–26]. As for $LaNiO_{3-\delta}$, this phenomenon was firstly interpreted in terms of the transition from localized to itinerant state of σ^* electrons [25,26]. Later, however, the apparent "semiconductor to metal" transition was attributed to decreasing hole concentration due to extensive oxygen losses from the lattice on heating [22–24], although no direct experimental proof for this hypothesis can still be found in literature. Note that similar phenomena are quite typical for perovskite-type oxides, such as La(Ni,Ga)$O_{3-\delta}$ [10]. As for heavily doped $LaNi_{1-x}Ga_xO_{3-\delta}$ perovskites [7,19], oxygen permeation through La_2NiO_4-based ceramics is significantly affected by the surface exchange; the bulk ionic transport in $La_2NiO_{4+\delta}$ occurs by a complex mechanism, combining vacancy diffusion in the perovskite planes and interstitial anion migration in the rock-salt layers [8,9].

Continuing our studies on lanthanum nickelate-based mixed conductors [7–11,19], the present work is focused on the evaluation of electronic transport mechanisms and low-$p(O_2)$ stability limits of a series of Ni-containing phases, derived from $LaGa_{0.65}Mg_{0.15}Ni_{0.20}O_{3-\delta}$ perovskite and $La_2NiO_{4+\delta}$ with K_2NiF_4-type structure. In order to assess effects of acceptor- and donor-type doping, four compositions doped with lower- and higher-valence cations were selected, namely $La_{0.90}Sr_{0.10}Ga_{0.65}Mg_{0.15}Ni_{0.20}O_{3-\delta}$, $La_{0.50}Pr_{0.50}Ga_{0.65}Mg_{0.15}Ni_{0.20}O_{3-\delta}$, $La_2Ni_{0.8}Cu_{0.2}O_{4+\delta}$ and $La_2Ni_{0.9}Co_{0.1}O_{4+\delta}$. In combination with the results on oxygen permeation partly published earlier [8,9,19], data on phase stability limits are necessary to identify perspective directions for membrane materials development.

2. Experimental

Powders of $La_2Ni_{0.9}Co_{0.1}O_{4+\delta}$, $La_{0.90}Sr_{0.10}Ga_{0.65}Mg_{0.15}Ni_{0.20}O_{3-\delta}$ and $La_{0.50}Pr_{0.50}Ga_{0.65}Mg_{0.15}Ni_{0.20}O_{3-\delta}$ were obtained by a standard ceramic route from stoichiometric amounts of high-purity oxides or metal salts (nitrates and carbonates). Solid-state reactions were conducted in air at 1420–1630 K for 30–40 h with multiple intermediate grindings. In the case of $La_2Ni_{0.8}Cu_{0.2}O_{4+\delta}$, sintering of dense ceramic samples from the powders prepared by the conventional ceramic technique was hampered due to a liquid phase formation at relatively low temperatures, 1550–1600 K. In order to decrease the sintering temperature, an active powder of $La_2Ni_{0.8}Cu_{0.2}O_{4+\delta}$ was synthesized by the glycine-nitrate process (GNP), a self-combustion method using glycine as a fuel and nitrates of metal components as oxidant [27]. In the course of GNP, glycine was added in aqueous nitrate solution containing metal cations in the stoichiometric proportions; the glycine/nitrate molar ratio, calculated assuming that the only gaseous products of reaction are H_2O, CO_2, and N_2, was 1:1. Then the solution was heated until evaporation of enough water to initiate a self-sustaining reaction. The resultant powder was ball-milled and calcined at 1073 K for 2 h.

Dense ceramic samples were pressed at 270–400 MPa and sintered in air for 2–5 h. The sintering temperature was 1503 ± 5 K for $La_2Ni_{0.8}Cu_{0.2}O_{4+\delta}$, 1723 ± 5 K for $La_2Ni_{0.9}Co_{0.1}O_{4+\delta}$, and 1798 ± 5 K for $La_{0.90}Sr_{0.10}Ga_{0.65}Mg_{0.15}Ni_{0.20}O_{3-\delta}$ and $La_{0.50}Pr_{0.50}Ga_{0.65}Mg_{0.15}Ni_{0.20}O_{3-\delta}$ ceramics. After sintering, samples were annealed in air at 1273 K for 3–4 h and then slowly cooled in order to achieve equilibrium with air at low temperatures. The density of ceramics, determined by standard picnometric technique, was 96–98% of theoretical density calculated from results of X-ray diffraction (XRD) studies (Table 1).

General characterization of the materials included XRD, scanning electron microscopy combined with energy dispersive spectroscopy (SEM/EDS), dilatometry, determination of steady-state oxygen permeation fluxes, and faradaic efficiency studies; description of the experimental procedures and equipment was published elsewhere (Refs. [7–10,28] and references cited). The cells for the oxygen permeation and faradaic efficiency measurements [28] were made of yttria-stabilized zirconia (YSZ) and consisted of three separate parts: an oxygen pump, a sensor and YSZ ring which separated the pump and sensor; each part was fabricated independently and then sealed into a single cell. This construction was chosen in order to prevent the voltage applied to the electrodes of the oxygen pump and/or the sample affecting the sensor e.m.f. reading; this was checked after assembling the cells. The cells were also checked for gas leakages by sealing another oxygen

Table 1
Properties of ceramics

Composition	Relative density (%)	Space group	Unit cell parameters				Average TEC	
			a (nm)	b (nm)	c (nm)	α (deg)	T (K)	$\bar{\alpha} \times 10^6$ (K^{-1})
$La_2Ni_{0.8}Cu_{0.2}O_{4+\delta}$	98.1	$I4/mmm$	0.3858(0)	—	1.2787(3)	—	400–1240	13.3±0.1
$La_2Ni_{0.9}Co_{0.1}O_{4+\delta}$	96.2	$I4/mmm$	0.3871(1)	—	1.2656(5)	—	400–1265	12.8±0.1
$La_{0.90}Sr_{0.10}Ga_{0.65}Mg_{0.15}Ni_{0.20}O_{3+\delta}$	96.4	$R\bar{3}c$	0.5485(1)	—	—	60.56(5)	373–773	12.0±0.1
							773–1273	18.4±0.1
$La_{0.50}Pr_{0.50}Ga_{0.65}Mg_{0.15}Ni_{0.20}O_{3+\delta}$	96.0	$Pbnm$	0.5477(2)	0.5481(5)	0.7756(7)	—	373–923	9.2±0.1
							923–1273	14.5±0.1

pump onto the cells and simulating known oxygen-permeation fluxes. The total oxygen-leakage currents did not exceed 10 μA, which is less than 0.2% of the measured permeation fluxes. Data on oxygen permeability presented in this paper corresponds to the membrane feed-side oxygen partial pressure (p_2) equal to 21 kPa (atmospheric air). The faradaic efficiency results were obtained in air under zero oxygen chemical potential gradient.

The total electrical conductivity (4-probe DC) and Seebeck coefficient were measured as functions of the oxygen partial pressure varying in the range from 10^{-18} Pa to 50 kPa at 973–1223 K, and also separately at 300–1273 K in atmospheric air. The isothermal measurements vs. $p(O_2)$ were performed simultaneously on two bar-shaped ceramic samples placed in an YSZ cell comprising an electrochemical oxygen pump and a sensor, separated by glass–ceramic sealant; the experimental technique was described elsewhere [29,30]. The sample for thermopower measurements was placed along the natural temperature gradient in the cell (approximately 15 K/cm). Two Pt/Rh–Pt thermocouples were attached to the butt ends of the sample using Pt foil; the Pt leads of thermocouples served also as thermovoltage probes. The results of the Seebeck coefficient measurements were hence corrected for the contribution of platinum. For the total conductivity measurements, the second sample was placed in an isothermal plane of the same cell, in a crosswise orientation near the middle of the sample for Seebeck coefficient studies. At the start of the experiment, the cell was evacuated with a vacuum pump, filled with a mixture of O_2 and CO_2 (50:50), and then hermetically sealed in the cold zone of the device. In the course of measurements, the oxygen partial pressure was varied by the solid-electrolyte oxygen pump, continuously pumping oxygen in or out the cell, and controlled by the sensor. The criteria for equilibration of a sample after a change in either oxygen pressure or temperature included the relaxation rates of the conductivity and Seebeck coefficients less than 0.05%/min and 0.001 μV/K min, respectively. Due to possible compositional instabilities at oxygen partial pressures from 10^{-1} down to 10^{-6}–10^{-4} Pa, which result in hysteresis phenomena and, possibly, nonequilibrium values of the conductivity and Seebeck coefficient, in the present paper this $p(O_2)$ range is excluded from consideration. At higher and lower $p(O_2)$ values the transport properties were found completely reproducible, within the limits of standard experimental error.

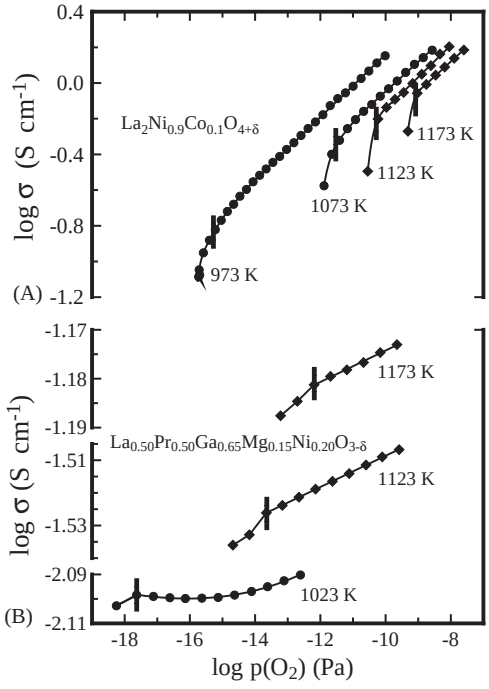

Fig. 1. Determination of phase stability limits of $La_2Ni_{0.9}Co_{0.1}O_{4+\delta}$ (A) and $La_{0.50}Pr_{0.50}Ga_{0.65}Mg_{0.15}Ni_{0.20}O_{3-\delta}$ (B) from the data on total conductivity. The stability boundaries are shown as dashed lines.

The phase stability boundaries of ceramic materials at low $p(O_2)$ were estimated from the results on total conductivity (σ) and Seebeck coefficient (α) as illustrated by Figs. 1 and 2, correspondingly. The oxygen pressure, at which the slope of $\log(\sigma)-\log p(O_2)$ and $\alpha - \log p(O_2)$ dependencies starts to change, was considered as the stability limit at a given temperature. Further reducing of oxygen partial pressure leads to drastic degradation of the electrical properties due to

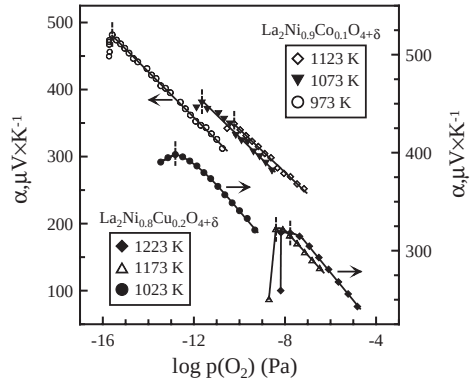

Fig. 2. Determination of $La_2Ni_{0.9}Co_{0.1}O_{4+\delta}$ and $La_2Ni_{0.8}Cu_{0.2}O_{4+\delta}$ phase stability limits from the data on Seebeck coefficient. The stability boundaries are shown as dashed lines.

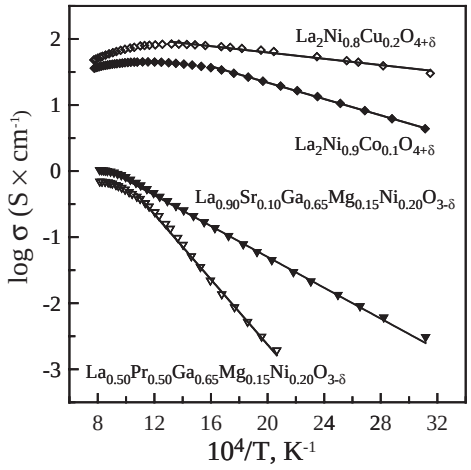

Fig. 3. Temperature dependence of the total conductivity of Ni-containing materials in air.

phase decomposition. The low-$p(O_2)$ stability limits presented in this paper are averaged from the results on Seebeck coefficient and total conductivity.

3. Results and discussion

3.1. Materials characterization

XRD analysis of $La_2Ni_{0.8}Cu_{0.2}O_{4+\delta}$ and $La_2Ni_{0.9}Co_{0.1}O_{4+\delta}$ ceramics showed formation of single phases with tetragonal K_2NiF_4-type structure, in agreement with literature [20–26]. For $La_{0.90}Sr_{0.10}Ga_{0.65}Mg_{0.15}Ni_{0.20}O_{3-\delta}$ and $La_{0.50}Pr_{0.50}Ga_{0.65}Mg_{0.15}Ni_{0.20}O_{3-\delta}$, the structure is perovskite-type with rhombohedral and orthorhombic distortions, respectively. The unit cell parameters calculated from XRD data are listed in Table 1. SEM/EDS analysis confirmed that the porosity of ceramics is low and that the cation distribution is homogeneous within the limits of experimental accuracy of the EDS method.

The average thermal expansion coefficients, calculated from dilatometric data in air, vary in the range $(9.2–18.4)\times10^{-6}\,K^{-1}$ (Table 1). Thermal expansion of $La_2Ni_{0.8}Cu_{0.2}O_{4+\delta}$ and $La_2Ni_{0.9}Co_{0.1}O_{4+\delta}$ ceramics at 400–1270 K is approximately linear. The dilatometric curves of perovskite ceramics exhibit a significant nonlinearity at temperatures above 770–920 K, which is associated, most probably, with extensive oxygen losses on heating.

Fig. 3 presents the temperature dependencies of the total conductivity of Ni-containing materials in air; the corresponding values of activation energy (E_A), calculated by the standard Arrhenius model

$$\sigma = \frac{A_0}{T}\exp\left(-\frac{E_A}{RT}\right), \quad (1)$$

where A_0 is the pre-exponential factor, are listed in Table 2. At temperatures below 870 K, $La_2Ni_{0.8}Cu_{0.2}O_{4+\delta}$ and $La_2Ni_{0.9}Co_{0.1}O_{4+\delta}$ exhibit a semiconductor-type behavior. In agreement with literature data [22–26], an apparent transition to pseudometallic conduction is observed at higher temperatures. For perovskite-type phases, the conductivity tends to a similar transition above 930–1120 K (Fig. 3). This behavior is discussed below using the data on $p(O_2)$ dependencies of the total conductivity and Seebeck coefficient.

3.2. Phase stability

The phase stability limits of Ni-containing compounds evaluated from data on the total conductivity and Seebeck coefficient are shown in Fig. 4A; Fig. 4B compares the stability boundary of $La_2Ni_{0.9}Co_{0.1}O_{4+\delta}$ with literature data on binary metal oxides [31] and La_2NiO_4 [32]. Phase decomposition of $La_2Ni_{0.8}Cu_{0.2}O_{4+\delta}$ and $La_2Ni_{0.9}Co_{0.1}O_{4+\delta}$ occurs at oxygen partial pressures substantially lower than that of NiO. A similar enlargement of the stability domain was earlier reported for K_2NiF_4-type $La_2CuO_{4+\delta}$ [33], though in the latter case the decomposition mechanism is more complex than a single-step reduction into transition metal and lanthanum oxide. The phase boundary of $La_2Ni_{0.8}Cu_{0.2}O_{4+\delta}$ is slightly shifted towards higher oxygen chemical potentials if compared to $La_2Ni_{0.9}Co_{0.1}O_{4+\delta}$; this seems reasonable since the equilibrium oxygen pressures over Cu_2O/CuO and Cu/Cu_2O mixtures are considerably higher with respect to Ni/NiO and Co/CoO. Nevertheless, the low-$p(O_2)$ stability limits of $La_2Ni_{0.8}Cu_{0.2}O_{4+\delta}$ and $La_2Ni_{0.9}Co_{0.1}O_{4+\delta}$ are very similar, also close to the phase boundary of undoped $La_2NiO_{4+\delta}$ at temperatures above 1173 K [32]. Hence, partial substitution of nickel with other transition metal cations, having either higher or lower oxidation state, has a minor effect on the stability of $La_2NiO_{4+\delta}$ at reduced $p(O_2)$.

Table 2
Parameters of Arrhenius model for the total conductivity and electron–hole mobility

Composition	Total conductivity		Electron-hole mobility	
	T (K)	E_A (kJ/mol)	T (K)	E_A (kJ/mol)
$La_2Ni_{0.8}Cu_{0.2}O_{4+\delta}$	320–760	8.6±0.1	1073–1223	12.6±1.2[a]
$La_2Ni_{0.9}Co_{0.1}O_{4+\delta}$	300–625	15.4±0.1	973–1223	14.5±0.7[a]
$La_{0.90}Sr_{0.10}Ga_{0.65}Mg_{0.15}Ni_{0.20}O_{3+\delta}$	300–1123	26.6±0.6	—	—
$La_{0.50}Pr_{0.50}Ga_{0.65}Mg_{0.15}Ni_{0.20}O_{3+\delta}$	480–930	52.8±1.2	1023–1223	39.4±4.6[b]

[a] $\delta = 0.19$.
[b] Oxidizing conditions ($p(O_2) = 20$–$40{,}000$ Pa).

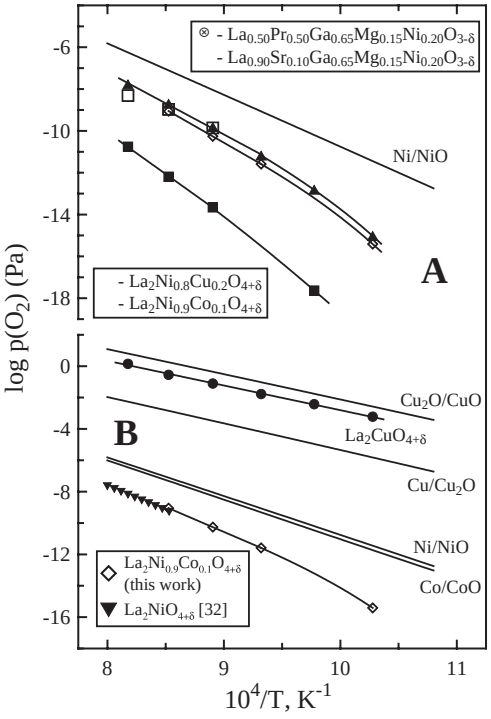

Fig. 4. Phase stability limits of Ni-containing ceramics, determined from the data on total conductivity and Seebeck coefficient. Literature data on binary metal oxides [31], $La_2NiO_{4+\delta}$ [32] and $La_2CuO_{4+\delta}$ [33] are shown for comparison.

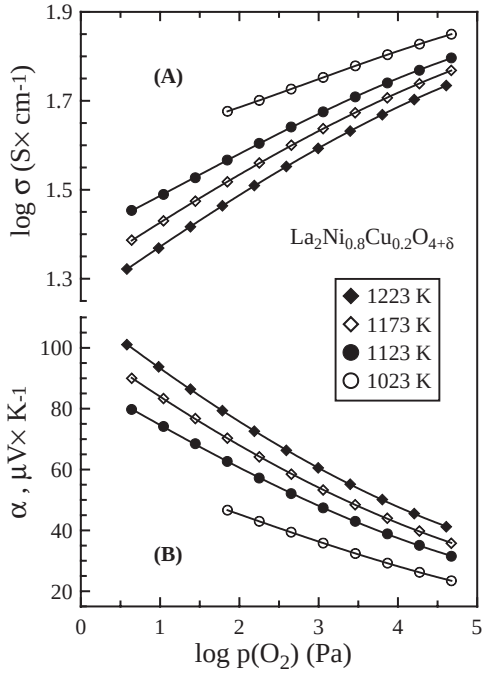

Fig. 5. Oxygen partial pressure dependence of the total conductivity (A) and Seebeck coefficient (B) of $La_2Ni_{0.8}Cu_{0.2}O_{4+\delta}$ in oxidizing conditions.

On the contrary, the perovskite-type $La_{0.50}Pr_{0.50}Ga_{0.65}Mg_{0.15}Ni_{0.20}O_{3-\delta}$ decomposes at oxygen partial pressures 10^2–10^4 times lower than $La_{0.90}Sr_{0.10}Ga_{0.65}Mg_{0.15}Ni_{0.20}O_{3-\delta}$ (Fig. 4A). Whilst the phase stability boundary of the latter is close to that of $La_2Ni(M)O_{4+\delta}$ (M = Co, Cu), the Pr-substituted perovskite is stable down to $p(O_2)$ values as low as 10^{-17}–10^{-10} Pa at 1023–1223 K. Most likely, such an enhancement results from increasing oxygen content due to incorporation of praseodymium cations, having the average oxidation state higher than 3+ and thus stabilizing the lattice. In the case of $La_{0.90}Sr_{0.10}Ga_{0.65}Mg_{0.15}Ni_{0.20}O_{3-\delta}$ in reducing conditions, nickel cations are expected to be mostly divalent, forming oxygen-deficient Ni–O octahedra in the lattice; this state is similar to La_2NiO_4-based solid solutions, leading to similar phase existence domains.

3.3. Electron–hole conductivity of La_2NiO_4-based phases

Figs. 5 and 6 present $p(O_2)$-dependencies of the electrical properties of $La_2Ni(M)O_{4+\delta}$ in oxidizing and reducing conditions, respectively. The total conductivity of nickelate ceramics decreases with decreasing oxygen pressure, while Seebeck coefficient has positive sign and increases. This unambiguously indicates that p-type electronic conduction dominates within the phase stability domain. One should note that the oxygen-ion transference numbers of La_2NiO_4-based phases in air, roughly estimated from the oxygen permeation data [8,9], are as low as 10^{-4}–10^{-2}. The permeation fluxes through $La_2Ni_{0.8}Cu_{0.2}O_{4+\delta}$ and $La_2Ni_{0.9}Co_{0.1}O_{4+\delta}$ membranes, presented below, suggest that the ion transference numbers are lower that 0.002. Although such estimates are crude due to surface-exchange

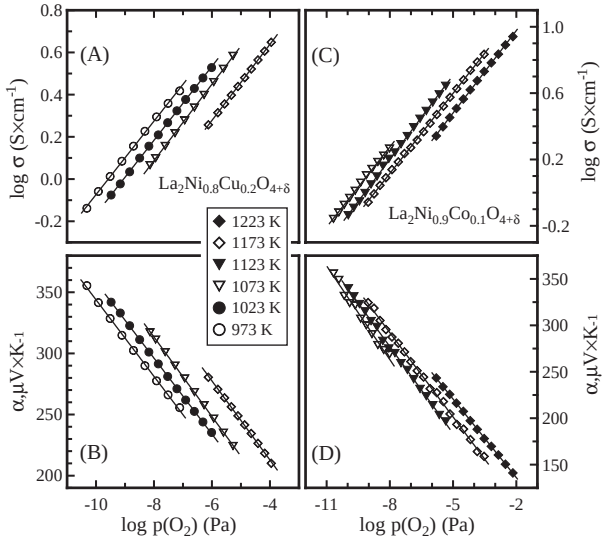

Fig. 6. Oxygen pressure dependencies of the total conductivity (A,C) and Seebeck coefficient (B,D) of $La_2Ni_{0.8}Cu_{0.2}O_{4+\delta}$ (A,B) and $La_2Ni_{0.9}Co_{0.1}O_{4+\delta}$ (C,D) in reducing conditions.

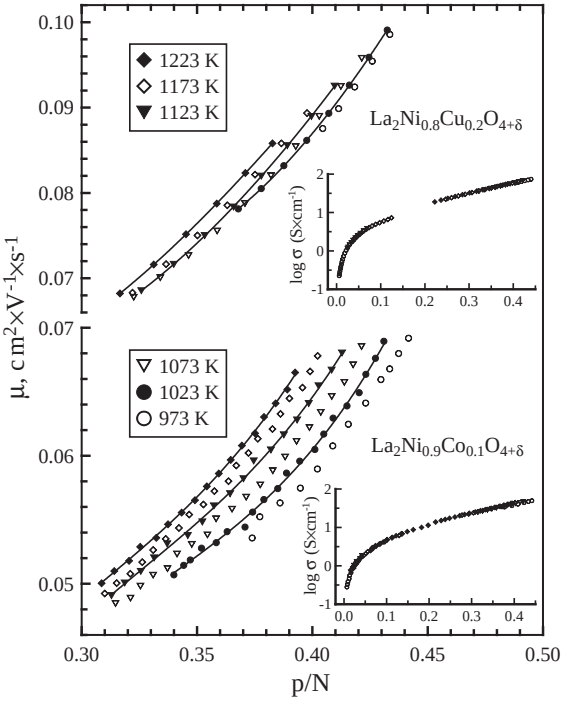

Fig. 7. Hole mobility in La_2NiO_4-based phases vs. relative hole concentration in oxidizing conditions. Insets show the total conductivity dependencies on (p/N) within the whole phase stability domain.

limitations of oxygen transport [6,8,9], these values undoubtedly show that the effect of ionic conduction on the total conductivity and Seebeck coefficient can be neglected. Moreover, due to significant interstitial-migration contribution to the ionic transport [8,9], the oxygen ionic conductivity of K_2NiO_4-type nickelates is expected to decrease with reducing $p(O_2)$.

In the range of high oxygen partial pressures, the $\log\sigma - \log p(O_2)$ and $\alpha - \log p(O_2)$ plots of $La_2Ni_{0.8}Cu_{0.2}O_{4+\delta}$ are nonlinear; the slope of these curves decreases with increasing oxygen pressure and with decreasing temperature (Fig. 5). Very similar behavior was observed for $La_2Ni_{0.9}Co_{0.1}O_{4+\delta}$. Such trends are in excellent agreement with literature data on $La_2NiO_{4+\delta}$, $La_{2-x}Sr_xNiO_{4+\delta}$ and $La_2Ni_{0.5}Cu_{0.5}O_{4+\delta}$ [4,34]. On the contrary, in reducing conditions the same dependencies become linear (Fig. 7), enabling an approximation by conventional power models, $\sigma \sim p(O_2)^{1/m}$ and $\exp(\alpha) \sim p(O_2)^{1/m}$; the regression parameters are listed in Table 3. The exponent, $1/m$, is quite close to the classical value of 1/6, which can easily be obtained considering a simple point-defect equilibrium in lanthanum nikelate. Assuming that the main point defects are interstitial oxygen ions (O_i'') and electron holes ($h^\bullet$), the oxygen incorporation process and corresponding equilibrium constant can be written as

$$\frac{1}{2}O_2 \Leftrightarrow O_i'' + 2h^\bullet, \quad K = \frac{[O_i'']p^2}{p(O_2)^{1/2}}, \tag{2}$$

where p is the concentration of electron holes. The simplified electroneutrality condition is

$$2[O_i''] = p. \tag{3}$$

If the hole mobility (μ) is independent of p-type charge carrier concentration

$$\sigma = F\mu p = \sigma_p^0 p(O_2)^{1/6}, \tag{4}$$

where σ_p^0 is a constant depending on temperature (Table 3). Note that the latter assumption is valid for a small-polaron conduction mechanism when the charge carrier concentration is low.

Within the entire stability domain at 973–1223 K, the total conductivity of $La_2Ni_{0.8}Cu_{0.2}O_{4+\delta}$ and $La_2Ni_{0.9}Co_{0.1}O_{4+\delta}$ decreases when temperature increases, thus showing a pseudometallic behavior (Figs. 5 and 6). However, taking the extensive oxygen-nonstoichiometry variations [4,22–24] into account, the electrical properties should be considered as a function of temperature at a fixed hyperstoichiometry or fixed concentration of the charge carriers. The hole concentration was estimated from the Seebeck coefficient by the Heikes formula [35–39], assuming that the ionic contribution to thermopower is negligible and that the conduction occurs via a hopping mechanism:

$$\alpha = \frac{R}{F}\left(\ln\frac{\beta(N-p)}{p} + \frac{q}{RT}\right), \tag{5}$$

where N is the total concentration of sites participating in the conduction mechanism, β is a factor due to spin and orbital degeneracy, and q is the transported heat of holes. For $La_2Ni_{0.8}Cu_{0.2}O_{4+\delta}$ and $La_2Ni_{0.9}Co_{0.1}O_{4+\delta}$, the value of N is supposed equal to the total B-site concentration, determined from XRD results. The

Table 3
Regression parameters of the power dependencies of total conductivity[a] and Seebeck coefficient[b] on the oxygen partial pressure in reducing conditions

Composition	T (K)	Total conductivity			Seebeck coefficient		
		m	σ_p^0 (S/cm)	ρ[c]	m	$b \times 10^5$, (V/K)	ρ
$La_2Ni_{0.8}Cu_{0.2}O_{4+\delta}$	1173	5.55±0.04	22.9±0.3	0.9999	6.1±0.2	8.4±0.4	0.9996
	1073	5.53±0.05	34.3±0.8	0.9999	6.10±0.06	5.3±0.2	0.9999
	1023	5.71±0.04	38.5±0.9	0.9999	6.39±0.06	4.7±0.2	0.9999
	973	5.7±0.2	49±5	0.9994	6.3±0.2	2.9±0.7	0.9995
$La_2Ni_{0.9}Co_{0.1}O_{4+\delta}$	1173	6.21±0.06	25.4±0.6	0.9999	6.6±0.1	5.0±0.4	0.9992
	1123	5.92±0.09	36±2	0.9997	6.4±0.1	2.8±0.5	0.9993
	1073	6.2±0.2	38±4	0.9994	5.8±0.4	[d]	0.9949
	973	5.75±0.05	79±4	0.9998	5.7±0.2	−6±1	0.9983

[a] Model for conductivity vs. oxygen pressure: $\sigma = \sigma_p^0 p(O_2)^{1/m}$.
[b] Model for Seebeck coefficient vs. oxygen pressure: $\alpha = -(R/F)(1/m)\ln p(O_2) + b$.
[c] ρ is the correlation coefficient.
[d] Parameter is statistically insignificant.

transported heat, q, which can be estimated from the temperature dependence of thermopower at fixed charge-carrier concentration, is very low and typically can be neglected [37,38]. Assuming $\beta = 1$ and neglecting q, appropriate handling of Eq. (5) gives the concentration of electron–holes.

The variations of total conductivity as a function of relative hole concentration (p/N) in $La_2Ni_{0.8}Cu_{0.2}O_{4+\delta}$ and $La_2Ni_{0.9}Co_{0.1}O_{4+\delta}$ are illustrated by insets in Fig. 7. As expected, the values of σ decrease with charge carrier concentration on reducing $p(O_2)$, exhibiting a drastic drop at low oxygen pressures when (p/N) and, thus, oxygen hyperstoichiometry become close to zero. Due to such behavior, quantitative estimations of the electron–hole mobility as $\mu = \sigma/(Fp)$ were possible only for oxidizing atmospheres. For the data obtained at low $p(O_2)$, mobility assessment failed due to low charge-carrier concentration and high resultant errors; in fact, the error in μ estimates was greater than the mobility variations with temperature.

The concentration dependence of the hole mobility in $La_2Ni_{0.8}Cu_{0.2}O_{4+\delta}$ and $La_2Ni_{0.9}Co_{0.1}O_{4+\delta}$ under oxidizing conditions is presented in Fig. 7. At fixed oxygen hyperstoichiometry when $p = \text{const}$, the mobility exhibits a temperature-activated character, unambiguously indicating a small polaron conduction mechanism. Moreover, μ values in both materials are lower than the characteristic threshold of about 0.1 $cm^2/V\,s$, believed to be a rough criterion to separate polaron and broad-band conductors. The increase in μ values with increasing p/N ratio is typical for perovskite-related phases under oxidizing conditions [30,40]. As for perovskite ferrites [30], such a behavior may be partly related to the lattice contraction with increasing δ, which leads to greater overlap of nickel and oxygen electron orbitals and, thus, to a stronger covalency of Ni–O–Ni bonds. The activation energy for hole mobility at 973–1223 K is similar to the E_A for total conductivity in the low-temperature range (Table 2), suggesting that the conduction mechanism is kept the same, independent of temperature. Another necessary comment is that at low $p(O_2)$, despite the low accuracy of μ estimates, the hole mobility level is about $(2.0–3.5) \times 10^{-2}\,cm^2/V\,s$ at 973–1223 K. These values seem to indicate that the small-polaron conduction mechanism in Cu- and Co-doped $La_2NiO_{4+\delta}$ is preserved within all phase stability domain.

3.4. Electron–hole transport in Ni-containing perovskites

The results on the total conductivity and Seebeck coefficient of $La_{0.50}Pr_{0.50}Ga_{0.65}Mg_{0.15}Ni_{0.20}O_{3-\delta}$ under oxidizing and reducing conditions are given in Figs. 8 and 9, respectively; the inset in Fig. 8 illustrates general trends of electrical properties in the whole $p(O_2)$ range. An analogous behavior was observed for $La_{0.90}Sr_{0.10}Ga_{0.65}Mg_{0.15}Ni_{0.20}O_{3-\delta}$ (Fig. 10). In general, the behavior of these perovskites in oxidizing atmospheres is quite similar to that of K_2NiO_4-type nickelates and suggests, in particular, a dominant role of p-type electronic conduction. When reducing $p(O_2)$ from 21 to 0.1 kPa, an apparent transition from semiconducting to pseudometallic conductivity character is observed (Figs. 8A and 10A). As for La_2NiO_4-based phases, this transition relates to variations in the oxygen nonstoichiometry and, consequently, electron–hole concentration; the conductivity model is discussed below.

The faradaic efficiency studies of Ni-containing perovskite phases showed a significant ionic contribution to the total conductivity, increasing with temperature (Table 4). Notice that, though the ion transference numbers (t_o) listed in Table 4 might be slightly underestimated due to the surface limitations of ionic transport, the faradaic efficiency data on

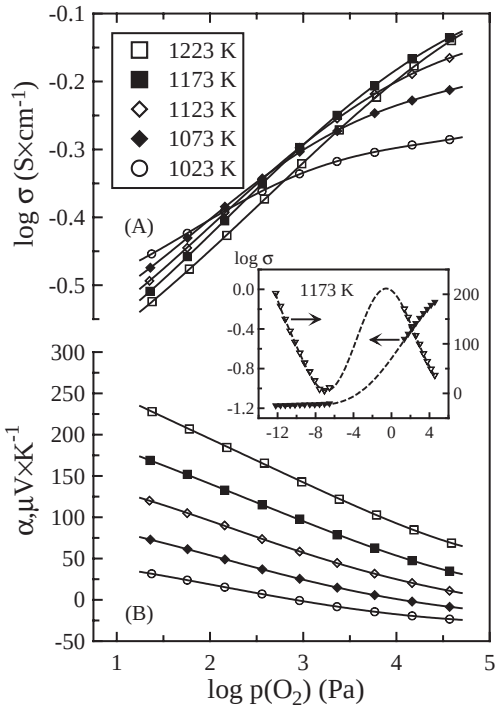

Fig. 8. Oxygen partial pressure dependence of the total conductivity (A) and Seebeck coefficient (B) of $La_{0.50}Pr_{0.50}Ga_{0.65}Mg_{0.15}Ni_{0.20}O_{3-\delta}$ in oxidizing conditions. Inset shows $p(O_2)$ dependence of the electrical properties in the whole studied $p(O_2)$ range.

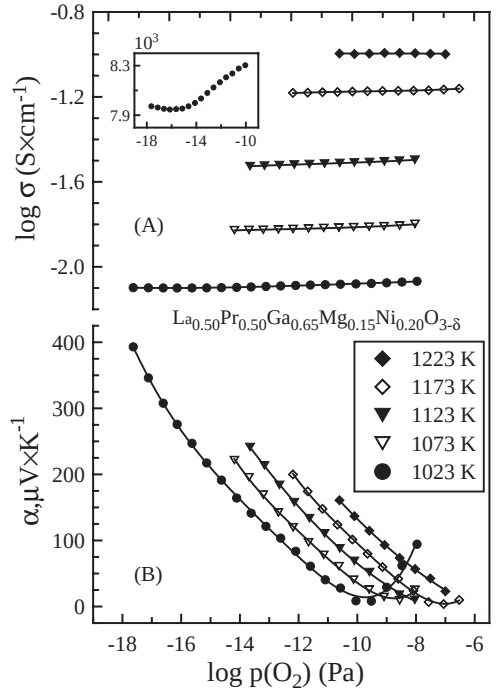

Fig. 9. Oxygen partial pressure dependence of the total conductivity (A) and Seebeck coefficient (B) of $La_{0.50}Pr_{0.50}Ga_{0.65}Mg_{0.15}Ni_{0.20}O_{3-\delta}$ in reducing conditions. Inset has a widen scale to illustrate conductivity behavior by the example at 1023 K.

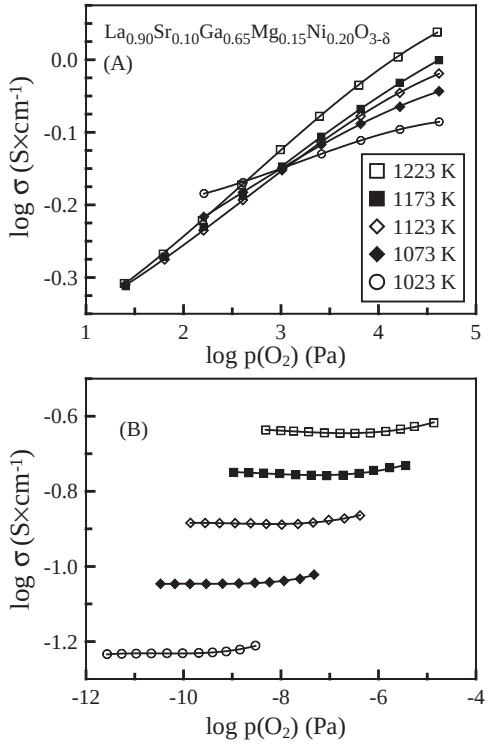

Fig. 10. Oxygen partial pressure dependence of the total conductivity of $La_{0.90}Sr_{0.10}Ga_{0.65}Mg_{0.15}Ni_{0.20}O_{3-\delta}$ in oxidizing (A) and reducing (B) conditions.

$LaGa_{0.65}Mg_{0.15}Ni_{0.20}O_3$-based ceramics are essentially surface-unaffected due to catalytically active porous Pt electrodes applied onto the membrane [7]. In addition, at 1173–1223 K the surface effect is, in any case, relatively small [7]. The oxygen ionic conductivity (σ_o) of the studied perovskites, heavily doped with acceptor cations, is expected to be $p(O_2)$-independent, at least, in a narrow oxygen pressure range. The ion transference numbers should therefore increase with reducing oxygen pressure due to decreasing p-type conduction.

Under oxidizing conditions when the n-type electronic conductivity is negligible, the total conductivity variations within a limited $p(O_2)$ range can be expressed as

$$\sigma = \sigma_o + \sigma_p^0 p(O_2)^{1/m}. \quad (6)$$

In this case, the Seebeck coefficient is a function of p-type electronic and oxygen-ionic contributions [38,39]

$$\alpha = t_o\alpha_O + (1 - t_o)\alpha_p = \frac{\sigma_o}{\sigma_o + \sigma_p^0 p(O_2)^{1/m}}\alpha_O + \frac{\sigma_p^0 p(O_2)^{1/m}}{\sigma_o + \sigma_p^0 p(O_2)^{1/m}}\alpha_p, \quad (7)$$

where α_O and α_p correspond to the partial thermopower of oxygen ions and electron holes, respectively. If equilibrium with gas phase is achieved and Soret effects are negligible, the partial ionic thermopower is

Table 4
Oxygen-ion transference numbers of Ni-containing perovskites, determined by the faradaic efficiency method in air

T (K)	$La_{0.50}Pr_{0.50}Ga_{0.65}Mg_{0.15}Ni_{0.20}O_{3-\delta}$	$La_{0.90}Sr_{0.10}Ga_{0.65}Mg_{0.15}Ni_{0.20}O_{3-\delta}$
1223	11.6×10^{-2}	14.4×10^{-2}
1173	6.8×10^{-2}	10.9×10^{-2}
1073	2.1×10^{-2}	—
973	4.8×10^{-3}	—

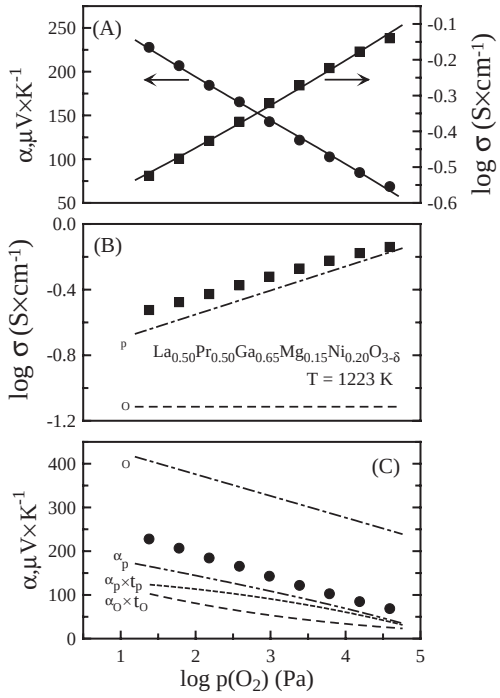

Fig. 11. Results of fitting experimental data on the total conductivity (σ) and Seebeck coefficient (α) of $La_{0.50}Pr_{0.50}Ga_{0.65}Mg_{0.15}Ni_{0.20}O_{3-\delta}$ in oxidizing conditions at 1223 K: (A) total conductivity and total thermopower; (B) calculated partial ionic and p-type electronic conductivities; (C) calculated partial ionic and hole thermopowers (α_O and α_p) and their contributions to total Seebeck coefficient ($t_o \times \alpha_O$ and $t_p \times \alpha_p$). t_p and σ_p are the electron–hole transference number and hole conductivity, respectively.

expressed as [39,41]:

$$\alpha_O = -\frac{R}{4F}\ln p(O_2) + \frac{1}{4F}\left[S^0_{O_2} - 2\left(\bar{S}_{O^{2-}} + \frac{q_{O^{2-}}}{T}\right)\right] = -\frac{R}{4F}\ln p(O_2) + \alpha^0_O, \quad (8)$$

where $S^0_{O_2}$ is the standard molar entropy of oxygen gas, $\bar{S}_{O^{2-}}$ is the partial molar entropy of mobile oxygen ions, $q_{O^{2-}}$ is the heat transported by oxygen ions, and α^0_O is the ionic thermopower at unit oxygen pressure. Combining Eqs. (4)–(7), assuming $\beta = 1$ and neglecting the transported heat of holes, one may obtain

$$\alpha_p = \frac{R}{F}\ln\left(\frac{NF\mu}{\sigma^0_p}p(O_2)^{-1/m} - 1\right), \quad (9)$$

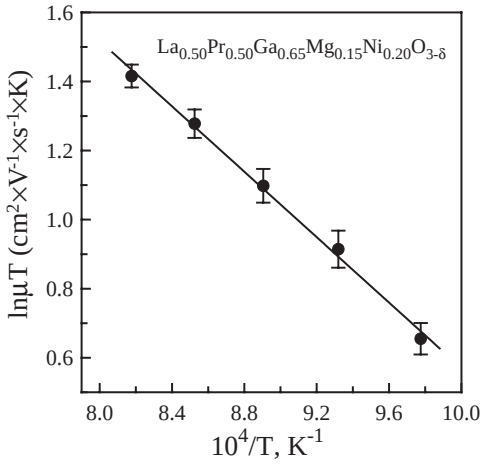

Fig. 12. Temperature dependence of the electron–hole mobility in $La_{0.50}Pr_{0.50}Ga_{0.65}Mg_{0.15}Ni_{0.20}O_{3-\delta}$ under oxidizing conditions.

where the hole mobility, μ, is supposed to be concentration-independent in a given $p(O_2)$ range. Eqs. (6)–(9) describe the total conductivity and Seebeck coefficient dependencies on oxygen partial pressure. This model was found adequate for $LaGa_{0.65}Mg_{0.15}Ni_{0.20}O_3$-based perovskites in oxidizing atmospheres assuming $p(O_2)$-independent ionic conductivity, with values determined from the faradaic efficiency results (Table 4). One example of fitting experimental data to this model is presented in Fig. 11A. Figs. 11B and C show partial contributions to the conductivity and thermopower, calculated from the fitting results.

The Arrhenius dependence of the hole mobility in $La_{0.50}Pr_{0.50}Ga_{0.65}Mg_{0.15}Ni_{0.20}O_{3-\delta}$, estimated from the data on total conductivity and Seebeck coefficient under oxidizing conditions, is given in Fig. 12. These estimates, obtained assuming that the p-type charge carriers are localized on nickel cations, should be understood as the upper limit of the hole mobility. If considering Pr sites available for hole hopping, the value of N in Eq. (9) increases and the hole mobility calculated from Seebeck coefficient decreases; however, this has no effect on the mobility activation energy. Notice also that the hole conductivity of $PrGaO_3$-based phases [42], where 100% A-sites are occupied with praseodymium ions, is 5–15 times lower than that of $La_{0.50}Pr_{0.50}Ga_{0.65}Mg_{0.15}Ni_{0.20}O_{3-\delta}$, suggesting a dominant contribution

of nickel cations. The temperature-activated character of the hole mobility in $La_{0.50}Pr_{0.50}Ga_{0.65}Mg_{0.15}Ni_{0.20}O_{3-\delta}$ (Fig. 12) indicates a small-polaron mechanism of the p-type transport, as for La_2NiO_4-based phases. The values of μ, varying in the range of $(1.8–3.4)\times10^{-3}$ cm^2/V s at 1023–1223 K, are considerably lower than that in $La_2Ni(M)O_{4+\delta}$. Such a behavior seems reasonable since hopping of p-type charge carriers in the *B* sublattice of $La_{0.50}Pr_{0.50}Ga_{0.65}Mg_{0.15}Ni_{0.20}O_{3-\delta}$ occurs between relatively isolated nickel cations, partly neighbored by Ga^{3+} and Mg^{2+} having the constant oxidation state. Similar phenomenon was earlier observed in $La_{0.3}Sr_{0.7}(Fe,Ga)O_{3-\delta}$ system [30]. Another difference with respect to the layered nickelates refers to the hole mobility activation energy, that is lower than E_A for total conductivity in the low-temperature range (Table 2). Most likely, this results from two simplifications, namely the assumptions regarding to $p(O_2)$-independent hole mobility and to the passive role of praseodymium cations. Despite these shortcomings, the obtained results unambiguously indicate that the p-type electronic transport in oxidizing atmospheres occurs via hopping mechanism.

3.5. Transport in Ni-containing perovskites under reducing conditions

At oxygen pressures lower than 10^{-7}–10^{-5} Pa, the total conductivity of $La_{0.50}Pr_{0.50}Ga_{0.65}Mg_{0.15}Ni_{0.20}O_{3-\delta}$ and $La_{0.90}Sr_{0.10}Ga_{0.65}Mg_{0.15}Ni_{0.20}O_{3-\delta}$ is weakly dependent of the oxygen partial pressure (Figs. 9A and 10B). In the case of Pr-containing composition at temperatures below 1050 K, the conductivity exhibits a small minimum, which might indicate a transition from p- to n-type electronic transport. For $La_{0.90}Sr_{0.10}Ga_{0.65}Mg_{0.15}Ni_{0.20}O_{3-\delta}$ a similar behavior is observed in the entire studied temperature range, 1023–1223 K. Such trend is illustrated by the inset in Fig. 9A where data on $La_{0.50}Pr_{0.50}Ga_{0.65}Mg_{0.15}Ni_{0.20}O_{3-\delta}$ at 1023 K are shown using one expanded scale to demonstrate total conductivity variations. However, the conductivity variations under reducing conditions are comparable to the level of experimental uncertainty. This may suggest that the ionic contribution to the total conductivity is dominant. In these conditions, Seebeck coefficient is expected to show a minimum at $p(O_2)$ values when the ionic contribution to the thermopower becomes prevailing with respect to the hole contribution, as described by Eqs. (7) and (8) and shown in Fig. 9B. Further decrease of the oxygen pressure leads to increasing absolute α values; the slope of $\alpha - \ln p(O_2)$ curves around the minimum is close to $(R/4F)$, characteristic of the dominant ionic conductivity independent of oxygen pressure (see Eq. (8)).

This conclusion is supported by the comparison of minimum total conductivity (σ_{min}) in reducing conditions and the oxygen ionic conductivity in air (Fig. 13). In the case of $La_{0.50}Pr_{0.50}Ga_{0.65}Mg_{0.15}Ni_{0.20}O_{3-\delta}$ at 1073–1223 K, the values of σ_{min} correspond to oxygen partial pressures slightly higher than the decomposition limits (Fig. 1); the ionic conductivity is calculated from faradaic efficiency results (Table 4). Within the studied temperature range, these quantities are close to each other and have very similar E_A values. For comparison, the activation energies for σ_{min} and σ_o of $La_{0.50}Pr_{0.50}Ga_{0.65}Mg_{0.15}Ni_{0.20}O_{3-\delta}$ are 146 ± 6 and 150 ± 3 kJ/mol, respectively. In the case of $La_{0.90}Sr_{0.10}Ga_{0.65}Mg_{0.15}Ni_{0.20}O_{3-\delta}$, E_A for the minimum total conductivity (80 ± 2 kJ/mol) is also close to the ionic conductivity activation energy of the Ni-free analogue, $La_{0.90}Sr_{0.10}Ga_{0.85}Mg_{0.15}O_{3-\delta}$, equal to 76.2 kJ/mol [43]. Therefore, at reduced oxygen pressure the ionic contribution to total conductivity of Ni-containing perovskites becomes dominant. At the same time, due to non-negligible electronic contribution resulting from intrinsic electronic disorder, σ_{min} values are slightly higher than σ_o (Fig. 13). Note that the latter difference may also be contributed by a minor increase of the ionic conductivity in reducing atmospheres. In air a significant part of nickel cations in the perovskite lattice exists as Ni^{3+} [10]; decreasing oxygen pressure converts them into divalent state, thus increasing oxygen-vacancy concentration and, possibly, affecting ionic conduction.

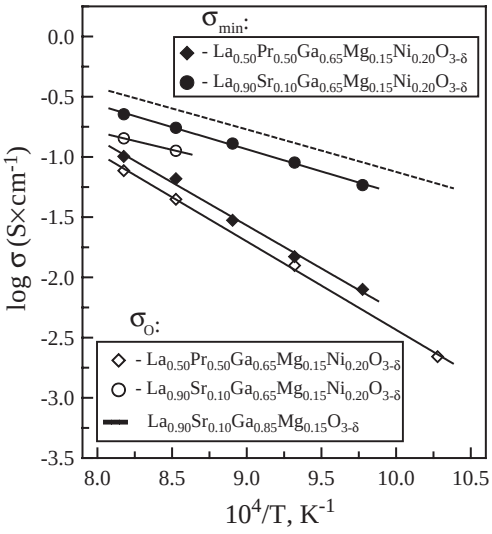

Fig. 13. Temperature dependence of the minimum total conductivity (σ_{min}) of Ni-containing perovskites under reducing conditions and the oxygen ionic conductivity (σ_o) in air. Data on $La_{0.90}Sr_{0.10}Ga_{0.85}Mg_{0.15}O_{3-\delta}$ [41] are shown for comparison.

3.6. Final comments

In order to assess the applicability of nickelate-based phases for oxygen membranes, Fig. 14 compares data on oxygen permeation through Ni-containing ceramics

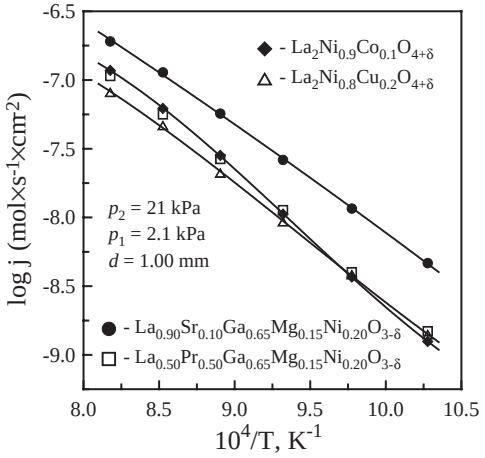

Fig. 14. Temperature dependence of oxygen permeation fluxes through Ni-containing ceramic membranes under fixed oxygen partial pressure gradient. Thickness of all membranes (d) is 1.00 mm.

under a fixed oxygen partial pressure gradient. Due to significant surface limitations to oxygen transport [6–9,19], all studied materials exhibit comparable level of oxygen permeability, except for $La_{0.90}Sr_{0.10}Ga_{0.65}Mg_{0.15}Ni_{0.20}O_{3-\delta}$. For the latter composition, the permeability is 2–3 times higher if compared to $La_{0.50}Pr_{0.50}Ga_{0.65}Mg_{0.15}Ni_{0.20}O_{3-\delta}$ and La_2NiO_4-based ceramics. At the same time, the phase stability of Sr-substituted perovskite and $La_2Ni(M)O_{4+\delta}$ under reducing conditions is similar, being insufficient for the operation under large oxygen chemical potential gradients, such as air/methane, at temperatures above 1000–1050 K (Fig. 4). In addition, $La_{0.90}Sr_{0.10}Ga_{0.65}Mg_{0.15}Ni_{0.20}O_{3-\delta}$ ceramics have a relatively high thermal expansion coefficient, $18.4\times10^{-6}\,K^{-1}$ at 773–1273 K, limiting the compatibility with other materials in the high-temperature zone of electrochemical reactors. This complicates the potential deposition of thin protective layers on the surface of $La_{0.90}Sr_{0.10}Ga_{0.65}Mg_{0.15}Ni_{0.20}O_{3-\delta}$ ceramics exposed to reducing atmospheres, which might improve the stability. Data on phase stability and oxygen permeation (Figs. 4 and 14) suggest that a better performance for the membrane applications may be achieved by incorporation of significant amounts of higher-valence cations, such as praseodymium, into the lattice of mixed-conducting perovskites. In particular, $La_{0.50}Pr_{0.50}Ga_{0.65}Mg_{0.15}Ni_{0.20}O_{3-\delta}$ ceramics possess a significant permeability, moderate TECs and an improved stability in reducing environments.

4. Conclusions

The electrical properties of a series of Ni-containing phases with K_2NiF_4- and perovskite-type structures were studied in the oxygen partial pressure range from 10^{-18} Pa to 50 kPa at 973–1223 K. Within the phase stability domain, the conductivity of La_2NiO_4-based materials is predominantly p-type electronic. Thermally activated mobility varying in the range of 0.02–0.10 $cm^2/V\,s$, and the $p(O_2)$ dependencies of total conductivity and Seebeck coefficient indicate a small-polaron conduction mechanism. The behavior of Ni-containing perovskites in oxidizing atmospheres is similar, but is characterized by a greater role of oxygen ionic conductivity. The ionic contribution to overall transport processes increases with increasing temperature or reducing $p(O_2)$, and becomes dominant at oxygen pressures below 10^{-7}–10^{-5} Pa. The apparent transition from semiconducting to pseudometallic conductivity behavior, observed for all nickelate-based materials at 870–1070 K, is due to decreasing electron–hole concentration, a result of oxygen losses on heating. The decomposition of Ni-containing phases occurs at low oxygen partial pressures with respect to the Ni/NiO boundary. Partial substitution of nickel with other transition metal cations, having either higher or lower oxidation state, has minor effect on the low-$p(O_2)$ stability limits of $La_2Ni(M)O_{4+\delta}$, which are similar to that of oxygen-deficient $La_{0.90}Sr_{0.10}Ga_{0.65}Mg_{0.15}Ni_{0.20}O_{3-\delta}$. On the contrary, praseodymium doping enhances the stability of $La_{0.50}Pr_{0.50}Ga_{0.65}Mg_{0.15}Ni_{0.20}O_{3-\delta}$ down to $p(O_2)$ values as low as 10^{-17}–10^{-10} Pa at 1023–1223 K. Such an enhancement may be advantageous for applications in oxygen-separation membranes, since all Ni-containing ceramics exhibit comparable level of oxygen permeability controlled by surface exchange.

Acknowledgments

This research was partially supported by the NATO Science for Peace program (project 978002), by INTAS (project 00276), by FCT, Portugal (POCTI program, and projects BPD/11606/2002 and BD/6595/2001), and by the Belarus Ministry of Education and Science.

References

[1] H.J.M. Bouwmeester, A.J. Burggraaf, in: A.J. Burggraaf, L. Cot (Eds.), Fundamentals of Inorganic Membrane Science and Technology, Elsevier, Amsterdam, 1996, pp. 435–528.
[2] T.J. Mazanec, Solid State Ionics 70/71 (1994) 11–19.
[3] P.N. Dyer, R.E. Richards, S.L. Russek, D.M. Taylor, Solid State Ionics 134 (2000) 21–33.
[4] V.V. Vashook, I.I. Yushkevich, L.V. Kokhanovsky, L.V. Makhnach, S.P. Tolochko, I.F. Kononyuk, H. Ullmann, H. Altenburg, Solid State Ionics 119 (1999) 23–30.
[5] S.J. Skinner, J.A. Kilner, Solid State Ionics 135 (2000) 709–712.
[6] B. Vigeland, R. Glenne, T. Breivik, S. Julsrud, Int. Patent Application PCT WO 99/59702, 1999.

[7] A.L. Shaula, A.P. Viskup, V.V. Kharton, D.I. Logvinovich, E.N. Naumovich, J.R. Frade, F.M.B. Marques, Mater. Res. Bull. 38 (2003) 353–362.
[8] V.V. Kharton, A.P. Viskup, E.N. Naumovich, F.M.B. Marques, J. Mater. Chem. 9 (1999) 2623–2629.
[9] V.V. Kharton, A.P. Viskup, A.V. Kovalevsky, E.N. Naumovich, F.M.B. Marques, Solid State Ionics 143 (2001) 337–353.
[10] A.A. Yaremchenko, V.V. Kharton, A.P. Viskup, E.N. Naumovich, N.M. Lapchuk, V.N. Tikhonovich, J. Solid State Chem. 142 (1999) 325–335.
[11] V.V. Kharton, A.A. Yaremchenko, A.V. Kovalevsky, A.P. Viskup, E.N. Naumovich, P.F. Kerko, J. Membr. Sci. 163 (1999) 307–317.
[12] V.V. Kharton, A.A. Yaremchenko, E.N. Naumovich, J. Solid State Electrochem. 3 (1999) 303–326.
[13] S. Primdahl, M. Mogensen, Solid State Ionics 152–153 (2002) 597–608.
[14] M. Schwartz, J.H. White, A.F. Sammells, Int. Patent Application PCT WO 97/41060, 1997.
[15] H.E. Höfer, R. Schmidberger, J. Electrochem. Soc. 141 (1994) 782–786.
[16] J.B. Goodenough, P.M. Raccah, J. Appl. Phys. 36 (1965) 1031–1032.
[17] J. Drennan, C.P. Tavares, B.C.H. Steele, Mater. Res. Bull. 17 (1982) 621–626.
[18] H.E. Höfer, W.F. Kock, J. Electrochem. Soc. 140 (1993) 2889–2894.
[19] A.L. Shaula, A.A. Yaremchenko, V.V. Kharton, D.I. Logvinovich, E.N. Naumovich, A.V. Kovalevsky, J.R. Frade, F.M.B. Marques, J. Membr. Sci., 2002, in press.
[20] M.J. Sayagués, M. Vallet-Regí, A. Caneiro, J.M. González-Calbet, Solid State Ionics 66 (1993) 21–26.
[21] H. Tamura, A. Hayashi, Y. Ueda, Physica C 216 (1993) 83–88.
[22] J.M. Bassat, P. Odier, J.P. Loup, J. Solid State Chem. 110 (1994) 124–135.
[23] K. Ishikawa, W. Shibata, K. Watanabe, T. Isonaga, M. Hashimoto, Y. Suzuki, J. Solid State Chem. 131 (1997) 275–281.
[24] S. Nishiyama, D. Sakaguchi, T. Hatori, Solid State Commun. 94 (1995) 279–282.
[25] J.B. Goodenough, S. Ramasesha, Mater. Res. Bull. 17 (1982) 383–390.
[26] Y. Takeda, R. Kanno, M. Sakano, O. Yamamoto, M. Takano, Y. Bando, H. Akinaga, K. Takita, J.B. Goodenough, Mater. Res. Bull. 25 (1990) 293–306.
[27] L.A. Chick, L.R. Pederson, G.D. Maupin, J.L. Bates, L.E. Thomas, G.L. Exarhos, Mater. Lett. 10 (1990) 6–12.
[28] V.V. Kharton, A.P. Viskup, E.N. Naumovich, N.M. Lapchuk, Solid State Ionics 104 (1997) 67–78.
[29] I.A. Leonidov, V.L. Kozhevnikov, E.B. Mitberg, M.V. Patrakeev, V.V. Kharton, F.M.B. Marques, J. Mater. Chem. 11 (2001) 1201–1208.
[30] M.V. Patrakeev, E.B. Mitberg, A.A. Lakhtin, I.A. Leonidov, V.L. Kozhevnikov, V.V. Kharton, M. Avdeev, F.M.B. Marques, J. Solid State Chem. 167 (2002) 203–213.
[31] V.N. Chebotin, M.F. Perfilyev, Electrochemistry of Solid Electrolytes, Khimiya, Moscow, 1978.
[32] D.E. Rice, D.J. Buttrey, J. Solid State Chem. 105 (1993) 197–210.
[33] H. Kanai, J. Mizusaki, H. Tagawa, S. Hoshiyama, K. Hirano, K. Fujita, M. Tezuka, T. Hashimoto, J. Solid State Chem. 131 (1997) 150–159.
[34] F. Mauvy, J.M. Bassat, E. Boehm, P. Dordor, J.P. Loup, Solid State Ionics 158 (2003) 395–407.
[35] R.R. Heikes, in: R.R. Heikes, R.W. Ure Jr.(Eds.), (Eds.), Thermoelectricity: Science and Engineering, Interscience, New York, 1961, p. 75.
[36] K. Kobayashi, S. Yamaguchi, T. Tsunoda, Y. Imai, Solid State Ionics 144 (2001) 123–132.
[37] J.B. Goodenough, in: N. Klein, D.S. Tannhauser, M. Pollak (Eds.), Conduction in Low-Mobility Materials, Taylor & Francis, London, 1971, pp. 87–100.
[38] E.O. Ahlgren, J. Ranløv, F.W. Poulsen, J. Electrochem. Soc. 142 (1995) 4230–4234.
[39] S. Yamaguchi, K. Kobayashi, K. Abe, S. Yamazaki, Y. Iguchi, Solid State Ionics 113–115 (1998) 393–402.
[40] E.B. Mitberg, M.V. Patrakeev, A.A. Lakhtin, I.A. Leonidov, V.L. Kozhevnikov, K.R. Poeppelmeier, J. Alloys Compd. 274 (1998) 103–109.
[41] H.T. Cahen, Bi_2O_3–M_2O_3 Systems: Structural, Electrical and Electrochemical Aspects, Ph.D. Thesis, Utrecht University, The Netherlands, 1980.
[42] P. Huang, A. Petric, W. Gong, in: T.A. Ramanarayanan (Ed.), Ionic and Mixed Conducting Ceramics III, The Electrochemical Society, Pennington, 1998, pp. 396–403.
[43] K. Huang, R.S. Tichy, J.B. Goodenough, J. Am. Ceram. Soc. 81 (1998) 2565–2575.